



APPLICATION OF A DISCONTINUOUS GALERKIN BASED CAA SOLVER FOR BROADBAND NOISE PREDICTION

Lev LIBERSON, Markus LUMMER, Michael MÖSSNER
Roland EWERT, Jan W. DELFS

*DLR, Abteilung Technische Akustik, Lillienthalplatz 7,
38114 Braunschweig, Deutschland*

SUMMARY

A recently developed CAA solver based on the discontinuous Galerkin (DG) method is used to compute the broadband noise generation of a five bladed axial fan. Sound propagation is predicted by the acoustic perturbation equations (APE) which are solved by the CAA solver on an unstructured tetrahedral grid. Acoustic sources are obtained by the Fast Random Particle Mesh (FRPM) method reconstructing synthetic turbulence from a previously obtained steady RANS turbulence statistics. The separation of the fluid mechanics from the acoustic simulation together with a source model based on synthetic turbulence reduces the computational effort thus providing a prospective tool for evaluation of low-noise based ventilator designs.

INTRODUCTION

Computational simulation forms an essential part in the development process of modern industrial fans. Computational fluid dynamics (CFD) is widely used for aerodynamic optimization thus leading to a fan design with improved efficiency. In addition, the acoustic performance becomes more and more important as a distinct product feature of high economic and environmental relevance. Especially for applications interfering with the human living environment, e.g. air conditioning technology or electronic hardware cooling, the demand for low-noise solutions is particularly high.

To obtain a low-noise fan design in a justifiable amount of time, efficient computational aeroacoustic (CAA) methods are necessary for the prediction of aerodynamically generated noise. While coming along with a high level of physical modeling, scale resolving simulations like e.g. Large Eddy Simulation (LES) are accompanied by a very extensive computational effort. On the other hand, fast approaches with a higher amount of modeling assumptions, i.e. empirical and semi-empirical models, are often restricted to very little deviations from the original design, thus having a limited applicability. To bridge the gap between high computational effort and low modelling inaccuracies, the development of a first principle based broadband fan noise prediction approach is

the aim of a co-operation between the industrial partner ebm-papst and the department of technical acoustics of the German Aerospace Center (DLR).

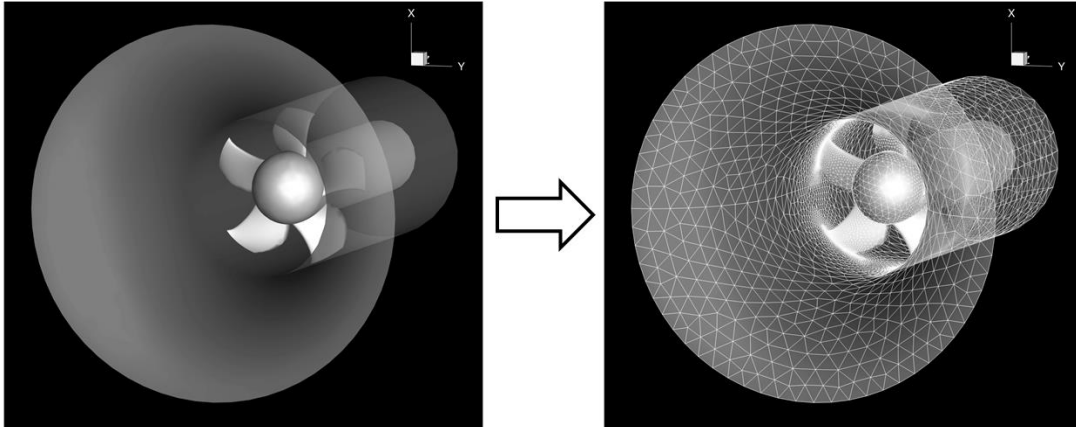


Figure 1: Complex 3-D geometry of a ducted axial fan discretized by an unstructured tetrahedral mesh. For clarity only surface meshing is depicted. Local refinement of element size is visible on the blades while coarsening is used at the inflow cone.

Recently, the CAA solver DISCO++ was developed at DLR for broadband noise assessment utilizing stochastically generated sources generated by the Fast Random Particle Mesh method (FRPM). In case of ventilator noise generation, three-dimensional flow effects play a significant role. Since also dealing with complex three-dimensional geometries an unstructured meshing approach for the computational domain is deemed to be beneficial. Local refinement often required due to small features of the geometry or high gradients in the flow field can be easily achieved using tetrahedral elements in an unstructured mesh. Fig. 1 depicts the surface mesh for a ducted axial fan, where various levels of refinement are used. The spatial discretization used by DISCO++ is based on the 4th order discontinuous Galerkin (DG) method to solve the acoustic perturbation equations (APE-4) [1].

The APE-4 represent a discretization of Pierce's exact wave equation [2] for irrotational flow in terms of a first order equation system formulated in primitive fluctuating variables, viz. pressure and velocity (p', \vec{v}'). Combined with appropriately derived vortex sound sources, an acoustic analogy is obtained based on the wave-equation of irrotational flow, akin to the Howe-Möhring acoustic analogy [3]. The applied APE-4 system in the rotating frame of reference is then given by

$$\begin{aligned} \frac{\partial p'}{\partial t} + c_0^2 \nabla \cdot \left(\rho_0 \vec{v}' + \vec{v}_0 \frac{p'}{c_0^2} \right) &= 0, \\ \frac{\partial \vec{v}'}{\partial t} + \nabla (\vec{v}_0 \cdot \vec{v}') + \nabla \left(\frac{p'}{\rho_0} \right) &= -\vec{L}'. \end{aligned} \quad (1)$$

The mean flow from (U)RANS is indicated with subscript '0'. In the rotating frame of reference, the mean flow is augmented by an additional velocity contribution from solid body rotation. To be precise, for a coordinate system with the x-axis equal to the fan rotor axis, it is $\vec{v}_0(\vec{x}) = \vec{v}_0^*(\vec{x}) - \vec{\Omega}_r \times \vec{x}$, where the asterisk denotes the mean flow velocity in a fixed frame of reference and the fan angular velocity is given by $\vec{\Omega}_r$. Note, the APE system appears to be invariant in form (or 'covariant') under general coordinate transformation, refer also to the discussion in [4]. For further discussion of this feature refer also to the CAA setup section below.

The main source term is the fluctuating Lamb vector $\vec{L}' = \vec{\omega}_0^* \times \vec{u}^t + \vec{\omega}^t \times \vec{v}_0^*$, with the turbulent velocity vector \vec{u}^t and its vorticity $\vec{\omega}^t$ being provided by FRPM and the mean flow velocity evaluated without the contribution from solid body rotation.

The test case investigated is well known as the “USI7” rotor which was designed and investigated at the University of Siegen to serve the purpose of a benchmark case for future studies on ventilator aerodynamics and acoustics. A detailed description of the setup as well as experimentally obtained data is provided by Carolus et al. [5] and is used within this study as reference. Furthermore, various numerical investigations of the assembly exist utilizing different numerical methods – e.g. a study based on LES performed by Pogorelov et al. [6] as well as Lattice-Boltzmann based simulations by Zhu et al. [7]. Those results can be used in a future work to further validate the DISCO++ - FRPM – method and compare the computational efficiency of the hybrid approach.

In the following course of the work, firstly the numerical method is presented. The acoustic source term generation via FRPM is explained along with the propagation code DISCO++. Next, a brief description of the computational setup of the simulated problem is given. Eventually, the results are discussed and juxtaposed against reference data.

NUMERICAL METHOD

The numerical approach applied to compute noise generation and propagation can be understood as a hybrid method comprising of two steps. In the first step, a solution of the flow problem is obtained by means of CFD. This can be performed by solving the Reynolds-averaged Navier-Stokes (RANS) equations in steady or unsteady form (URANS) or applying scale resolving methods, e.g. LES. In a subsequent step, the unsteady acoustic field is solved by a coupled run of the CAA solver DISCO++ and the FRPM code, which is used to reconstruct time resolved acoustic source terms based on the previous flow solution, i.e. the flow field and its turbulence statistics.

Stochastic sound source generation with FRPM

The Fast Random Particle Mesh method is implemented as a separated tool with the purpose of reconstructing unsteady, i.e. time resolved, fluctuating acoustic sources from a precomputed flow field solution [8]. Statistical turbulence information, such as the specific turbulent kinetic energy k_t and the specific turbulent dissipation ω , combined with the mean flow magnitudes (velocity vector \vec{u}_0 , pressure p_0 and density ρ_0) are used to generate synthetic turbulence, i.e. stochastic velocity fluctuations. The method directly provides the right hand side for a given set of acoustic propagation equations, such as the linearized Euler equations (LEE) or the acoustic perturbation equations (APE). In case of the APE the right-hand side is described by the perturbed Lamb vector \vec{L}' . A schematic of the workflow is provided in Fig. 2.

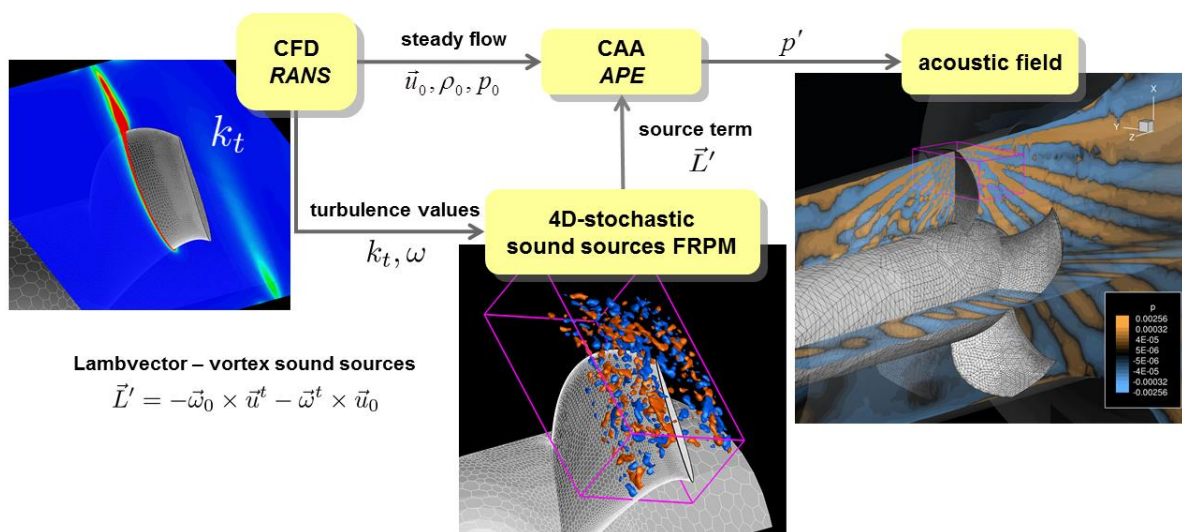


Figure 2: Diagram of the numerical method applied. Acoustic source terms are generated by FRPM based on turbulence statistic data from a flow solution. Together with mean flow quantities, the sources are used within the APE to describe the sound propagation.

The reconstruction process is done on a separate Cartesian grid which partially overlaps with the considered CAA domain. This way, the acoustic sources are only computed in a specified area, allowing an isolation of different noise generation mechanisms while also limiting the computational effort. The clear benefit of this approach over scale resolved simulation is to limit the fairly costly process of turbulence reconstruction to the actual area of noise generation.

Benefits of a hybrid CAA-CFD approach

By incorporating such an approach the low Mach number disparity in length scale between CAA and CFD is avoided to a certain extent. The CFD computation is performed on a grid especially designed for flow computation purposes, e.g. refinement is used to sufficiently resolve boundary layers while homogeneous areas in the flow can be discretized in a much coarser manner. The acoustic simulation is performed in a subsequent step using a grid optimized for acoustic purposes. Here, the highest frequency f_{\max} to be resolved determines the minimum size Δ_{\min} of the elements, which is typically far greater compared to the minimum length scales of the CFD computation. Since DISCO++ uses an explicit fourth-order-accurate Runge-Kutta time integration method, the minimum length scale is proportional to the applicable time step. Thus, an optimal CAA grid should not contain any cells smaller than required to properly resolve acoustic waves of the frequency f_{\max} for minimizing the computational effort. Coarsening can be used to reduce the overall element count while reducing the frequency resolution in the areas applied. Nonetheless, some non-acoustic driven refinement has to be done in most applications to ensure a proper discretization of geometric features. Those are e.g. leading and trailing edges of ventilator blades or narrow gaps between solid bodies. A further demand on the refinement of the CAA grid is posed by the usage of FRPM for the computation of acoustic sources, since subsonic acoustic sources are smaller than the acoustic waves they produce.

Propagation code DISCO++

The FRPM computation is coupled in the time domain to the CAA solver which computes the sound propagation based on the source terms provided. Those are interpolated from the FRPM domain onto the CAA grid. To ensure an accurate interpolation, i.e. minimal aliasing effects, the length scale of the spatial discretization on both meshes has to be similar. A local refinement is demanded in this region.

Spatial discretization within the propagation code DISCO++ is done by the discontinuous Galerkin method, which combines concepts of the Finite Volume method with those of a Finite Element approach. The computational domain is decomposed into non-overlapping, tetrahedral elements. The choice of tetrahedral elements allows for a quadrature-free implementation of the DG method. The effort of calculating integrals over the elements, as demanded by the method, can be avoided by introducing a reference element, to which all others are mapped. The integration is performed for the reference element during preprocessing, as for the simulation run, only a matrix-vector multiplication must be done instead, leading to a more efficient implementation [9].

Within the tetrahedral elements a polynomial *ansatz* is chosen to obtain a high-order representation of the variables from the APE. To form the polynomial basis, i.e. the shape functions, Lagrangian polynomials of degree $p = 3$ are chosen. Those are defined by 20 sampling points (nodes), placed in an equidistant manner along the tetrahedral edges and on the surfaces. Unlike with the Finite Element method, the shape functions are restricted to one element, so the variables can become discontinuous at inter-element boundaries. This feature of the DG method is a similarity with the Finite Volume method and is handled analogously by introducing a numerical flux. The flux is calculated between adjacent nodes of two elements using the state in the left and right element, thus providing a weak coupling. This leads to a highly local stencil, since only the solution from the direct neighbors is needed to perform a Runge-Kutta step. This feature makes the DG method very

suitable for code parallelization via domain decomposition for information only needs to be exchanged at the direct boundaries of adjacent domains.

DISCO++ is implemented using a hybrid parallelization concept. The aim is to efficiently employ computational resource within distributed memory systems, such as nodes in a computational cluster, while also taking advantage of the shared memory architecture inside each node, e.g. multicore CPU. The inter-node parallelization is realized via domain decomposition and information interchange between the processes by the Message Parsing Interface (MPI). Intra-node parallelization is achieved through multithreading – utilizing the OpenMP application programming interface.

SIMULATED TESTCASE

To validate the numerical method the noise generation and propagation of the USI7 fan is computed and compared to measurement data from the original study done by Carolus et al. [5]. The test case consists of a five bladed, low pressure axial fan placed in a duct with an attached nozzle. No geometry upstream the nozzle is considered within this study, thus effects related to influence from the large-scale environment as described in [10] by Sturm et al. are not meant to be captured.

Test case geometry

A two dimensional schematic of the test case geometry used for the numerical studies is depicted in Fig. 3. The axial fan is placed on a shaft while the whole assembly is encased by a cylindrical duct. The rotational speed of the fan is $n = 3000 \text{ rpm}$. An Air Movement and Control Association (AMCA) standardized nozzle is mounted to the inlet of the duct.

The fan rotor has a nominal diameter $d_{rot} = 300 \text{ mm}$, while the encasing tube is of similar diameter. One aim of the benchmark case is to evaluate the effect of a size variation of the tip gap, i.e. the clearance between the tip of a ventilator blade and the casing. Thus, the nominal rotor diameter is reduced in two steps by precision milling to achieve a gap of $s_{1\%} = 3.0 \text{ mm}$ and $s_{0.1\%} = 0.3 \text{ mm}$, respectively. For the numerical studies no further geometry, e.g. shaft mounting, was taken into consideration.

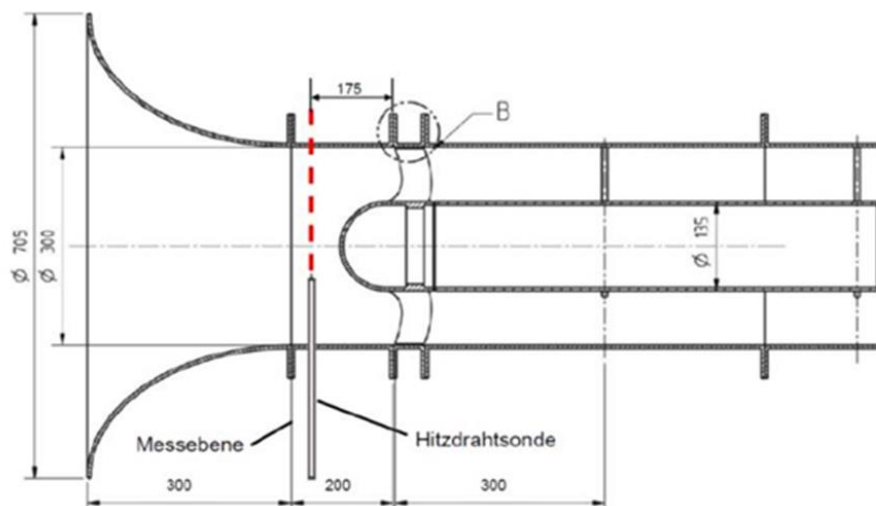


Figure 3: Schematic of the test case geometry.

CFD setup

The flow field for the test case is provided by the project partner ebm-papst and is treated solely as input; hence, no evaluation of the CFD quality is performed within this study. However, as the flow exhibits no separation it is well known that RANS provides a reliable input. The steady RANS

computation is performed utilizing the commercial CFD solver STAR-CCM+ by CD-adapco. To reduce the computational effort the periodicity of the geometry is exploited. As depicted in Fig. 4, a partial model, i.e. one fifth of the assembly, is used for the computational domain using periodic boundary conditions at the segment boundaries. The rotational movement of the rotor is not realized by actual moving geometry. Instead, the CFD domain is divided into a rotating and non-rotating part. The moving subdomain is then computed in a rotating frame of reference. Information between the subdomains is interchanged via sliding interfaces.

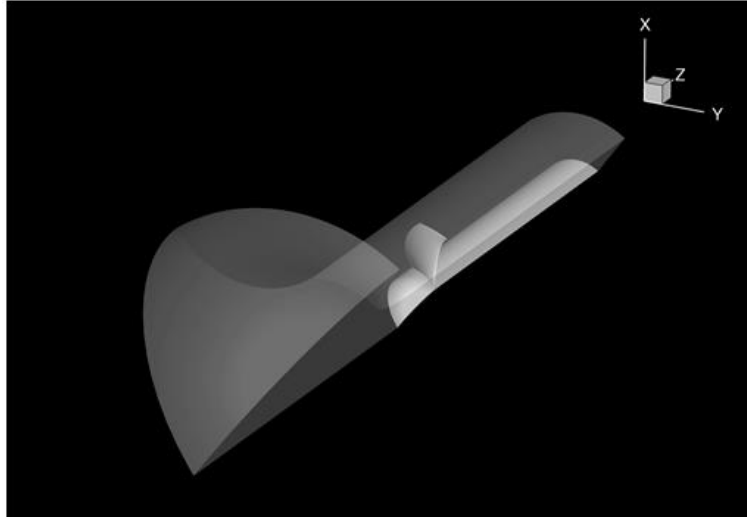


Figure 4: CFD-domain as used in the RANS computation. A partial model with periodic boundaries is used to save computational time.

CAA setup

For the datum problem the precomputed RANS mean flow solution does not account for any inflow disturbances upstream of the fan due to its geometrical restrictions. This allows reformulating the simulation problem in a rotating frame of reference, co-rotating with the fan with a constant angular velocity $\vec{\Omega}_r$. In this system fan, casing and mean flow are stationary. However, the no-slip condition at the casing walls transforms into a slip condition in the transformed system with a wall velocity defined by $\vec{\Omega}_r R$, where R indicates the radius of the casing. Furthermore, the solid body rotation $-\vec{\Omega}_r \times \vec{r}$ adds to the mean flow velocity used.

Because of the time dependent rotation of the triad defining the main coordinate directions in the rotating frame of reference, the coordinate transformation affects the vector components of the set of independent variables, i.e. the fluctuating velocity, but not scalar components (pressure). The extra term of the momentum equation that specifies the solution in the non-inertial frame of reference must be linear in the velocity fluctuations and furthermore depends linearly on the angular velocity.

The reasoning is completely equivalent to the transformation of e.g. the transport equations of fluctuating velocity into a rotating reference frame, yielding the same extra term also in the APE system, i.e. a Coriolis term $-2\vec{\Omega}_r \times \vec{v}'$; refer to the discussion of Speziale [11]. However, the mean vorticity term in the Lamb vector of the APE system provides an equivalent term on the right-hand side, noting that the coordinate system rotation provides an extra mean vorticity $-2\vec{\Omega}_r$ which in effect cancels the Coriolis term so that the APE system is invariant in form in a non-inertial coordinate system. Note, to comply with this formulation, the Lamb vector must be computed based on mean quantities from a fixed frame of reference, i.e. without contributions from solid-body rotation.

The CAA domain chosen for the test case is depicted in Fig. 5. A half ellipsoidal-shaped far field is placed upstream of the assembly to accommodate the virtual microphone positions. The radius of this zone is $R_{ff} = 1200 \text{ mm}$ while the length is $L_{ff} = 1880 \text{ mm}$, both given relative to the center of nozzle exit plane. Around the same point, the microphones are placed each ten degrees on a semicircle with the radius $R_{mic} = 1.0 \text{ m}$. Due to the rotating frame of reference, the sampling position of a microphone in the CAA domain is rotating. Thus, circles of 720 equidistant virtual microphones are placed on those paths and recorded simultaneously. A further post processing step is required to counteract the rotation, i.e. extract data for a fixed position in the non-rotating frame of reference.

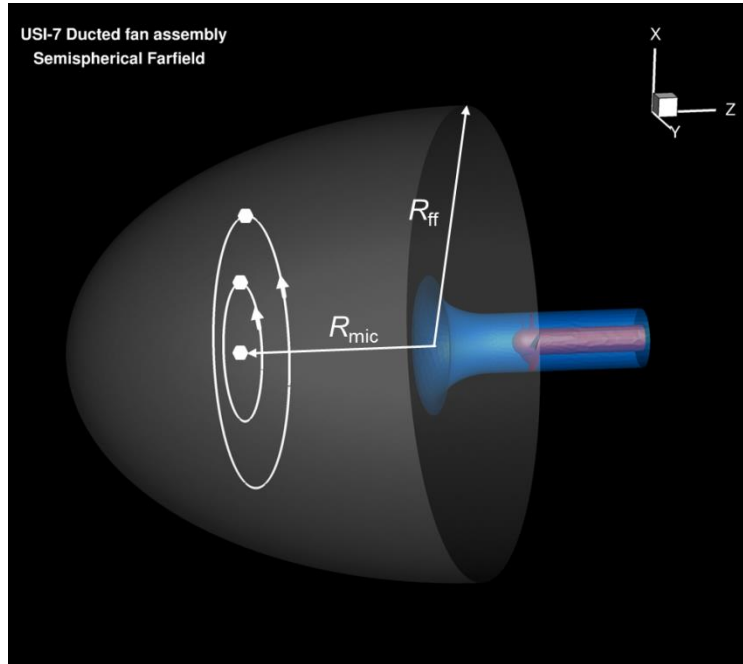


Figure 5: CAA-domain used for the acoustic simulations. Half ellipsoidal-shaped far field added to accommodate virtual microphones located along circles.

Though experimental data is provided for more positions, only three can be evaluated within the present CAA domain, i.e. $\varphi_{01} = 0^\circ$, $\varphi_{02} = 10^\circ$ and $\varphi_{03} = 20^\circ$. To facilitate the sampling of further microphones, i.e. $\varphi > 20^\circ$ the radius of the far field has to be extended. However, the azimuthal velocity component $v_{\theta,rot}$ is increasing linearly with the radius and surpasses the speed of sound, given by $c_0 = 343 \text{ m/s}$, above a certain radius. The radius, at which the sonic state, i.e. $Ma = 1$, is reached computes to $r_{Ma=1} = c_0/\omega_{rot} \approx 1.09 \text{ m}$. The current implementation of the APE system is not stable above $Ma = 1$, the computable far field radius is therefore limited. To facilitate a larger far field and thus reduce any possible influence of the boundaries, $v_{\theta,rot}$ is only allowed to increase in the range: $0 < r \leq 0.8 \text{ m}$. For any $r > 0.8 \text{ m}$ a fading function is applied to gradually reduce $v_{\theta,rot}$ to zero at the maximum radius of the far field $R_{ff} = 1200 \text{ mm}$.

Simulated configurations

In this study two variations of the tip gap are simulated, i.e. $s_{01\%} = 0.3 \text{ mm}$ and $s_{1\%} = 3.0 \text{ mm}$. The former is referenced to as case A1, the latter – case A2. An unstructured grid for each configuration is generated with the grid generator CENTAUR. For the A1 configuration, the tip gap is actually not resolved by the CAA grid, since very small element sizes are required – leading to extensive computational effort. Thus, the ventilator blades are in contact with the geometry of the encasement. Nonetheless, the impact of the gap on the noise generation of the ventilator is captured through the acoustic source terms computed by FRPM.

The FRPM domain, as depicted in Fig. 6, contains the flow and the turbulence statistic information from RANS simulations. In case of the CFD grid, the tip gap is fully resolved, thereby taking all flow phenomena in this region into account. The effect of not providing any CAA elements in the particular tip gap, thus not being able to receive the acoustic sources there, is believed to be negligible in the A1 case. This is justified partially due to the relatively small volume of the unresolved area and partially due to the nature of the acoustic source. The main mechanism of noise generation at the tip is believed to be a turbulent vortex, caused by the pressure compensation between the blades suction and pressure side. The interaction of the vortex and the blade geometry is deemed to be the main noise generation mechanism. However, the cardinal portion of the vortex is located outside of the tip gap area. To substantiate this hypothesis, the A2 case is simulated both with a resolved and an unresolved tip gap.

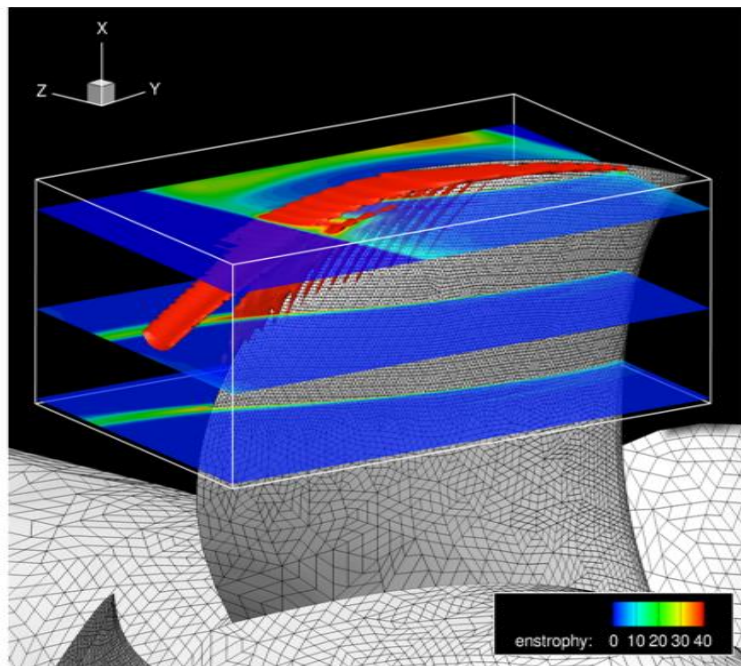


Figure 6: Rectangular domain of the FRPM source reconstruction around a ventilator blade. Tip gap vortex represented by slices and iso-surfaces of the enstrophy.

RESULTS

The instantaneous pressure field at the final time step of the simulation is presented in Fig. 7 for the A1 setup. The corresponding real time is $T_{real} = 89 \text{ ms}$. The two slices in the color plot show the pressure waves radiate spherically from the nozzle. Notably, acoustic sources are computed only for one of the five blades. The turbulence generated at each blade is stochastically independent of the others. Since, in case of the APE, a linear equation system is solved, the noise generation of the total assembly is the sum of five independent blades. To obtain the total pressure signal, a multiplication with the actual blade count is sufficient.

Furthermore, pressure patterns of various length scales can be observed. While structures of greater length, i.e. sound waves of lower frequency, are dominant, high frequency waves of lesser magnitude are also present. Those observations are confirmed by an evaluation of the sound pressure level spectra, as depicted in Fig. 8. Here, the sound pressure level recorded by the $\varphi_{01} = 0^\circ$ virtual microphone position is compared to corresponding experimental data. Since the achievable simulated time is much lower compared to the measurement, a higher value of Δf has to be used for the evaluation of the power spectral density.

Over a great range of frequencies the simulation is in good agreement with the measurement. However, at frequencies below approx. $f_{min} \approx 300 \text{ Hz}$, a discrepancy due to the short sampling

time of the simulation arises. The cut-off frequency of the CAA grid is at $f_{\max} \approx 8000$ Hz, which explains the strong decay of the amplitude further on. At frequencies higher than approx. $f \approx 4000$ Hz an over prediction of the signal of around 5 dB can be registered. It is deemed, that spurious noise is generated by the coupling of the CAA solver with the source generation method.

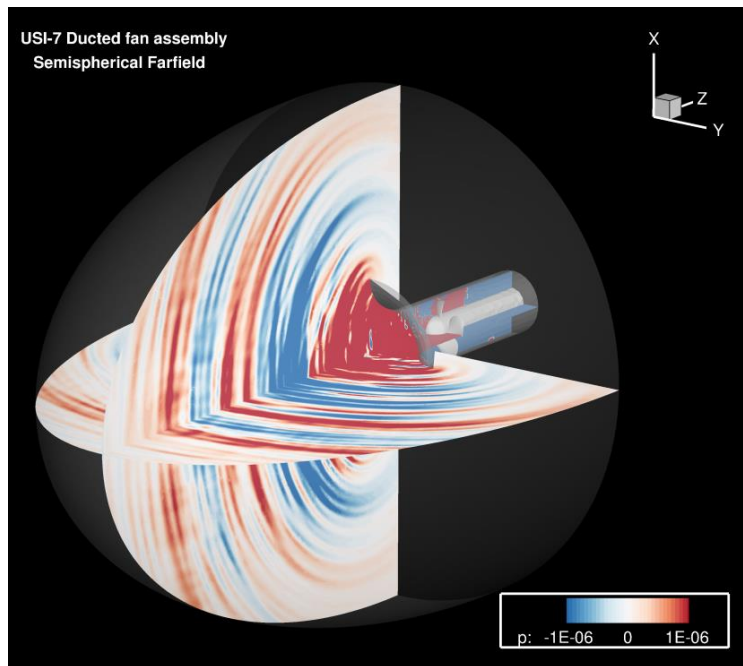


Figure 7: Color plot of the instantaneous pressure field for the case A1.

A further outstanding contrariness between measurement and simulation is the lack of the distinct tonal components in case of the numerical results which only reproduce the broad band part of the spectrum. The tonal components are believed to emerge from the periodic change in aerodynamic load on the fan blades caused by inflow disturbances. The formation of those is linked to the shape of the environment of the test rig [9]. However, in the present study, neither the CAA, nor the CFD domain do account for any geometry upstream of the ducted fan assembly. Thus, the tonal components of the measured spectra are not expected to be captured.

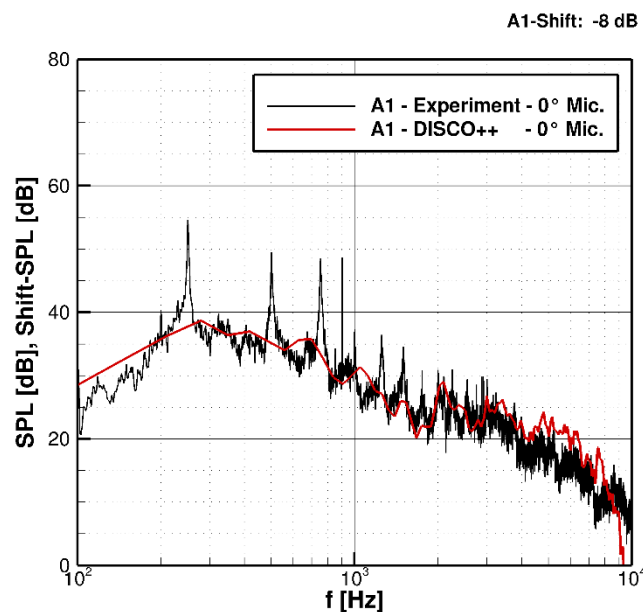


Figure 8: SPL spectra evaluated for axial microphone position, i.e. $\varphi_{01} = 0^\circ$. Simulated spectrum (red) is in good agreement with measurement (black) over a wide range of frequencies.

Similar assertions can be made for the $\varphi_{02} = 10^\circ$ microphone position, for which the spectrum is presented in the left portion of Fig. 9. As for the previous case, a good agreement in the shape of the spectrum can be found. For the $\varphi_{03} = 20^\circ$ microphone position, the simulation somewhat underpredicts the experimental spectrum in the region below approx. $f \approx 1000$ Hz.

Concerning the absolute sound pressure levels, the simulated signal has to be shifted down by $\Delta_{SPL} = -8$ dB by reason of the formulation of the acoustic sources used. No calibration to actual sound pressure levels is yet done. Nevertheless, the method allows for the prediction of deltas in sound pressure level for different configurations.

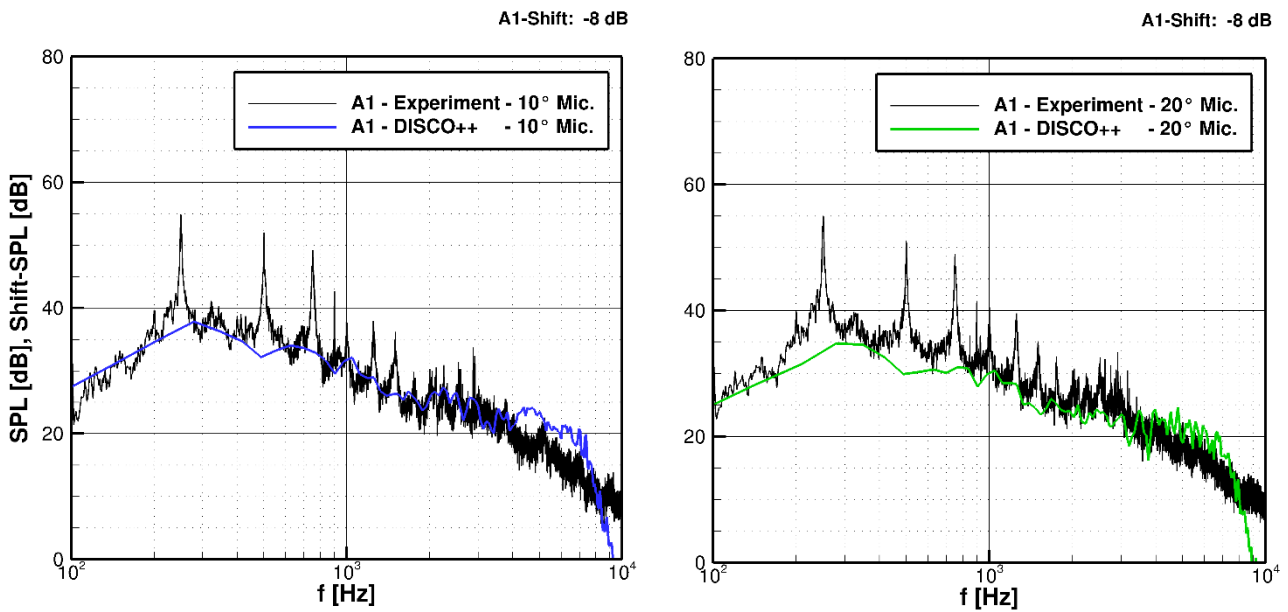


Figure 9: SPL spectra evaluated for microphone positions $\varphi_{02} = 10^\circ$ and $\varphi_{03} = 20^\circ$.

Though the general sound pressure level for the A2 configuration is higher as for the A1 case, the shape of the measured A2 spectrum is not reproduced to the same degree as before by the simulation, as depicted in Fig. 10. Especially in the mid-frequency range a lack of amplitude is prominent. An explanation could be the presence of unresolved effects in the CAA. The present level of acoustic grid refinement might not be sufficient enough, especially in the tip gap area.

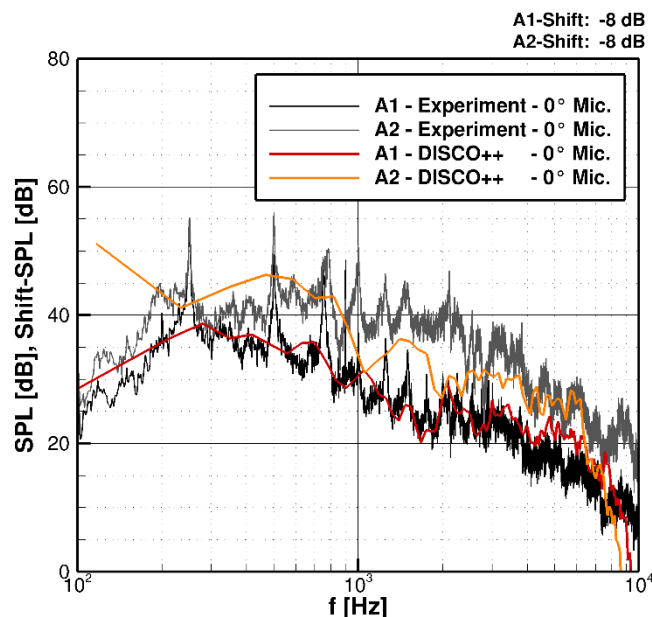


Figure 10: Comparison of small tip gap (A1) with large tip gap (A2) setup. Simulation underpredicts same increase in amplitude as found in experiment (black, grey) in mid frequency range.

To round off the result section the question whether not resolving the tip gap is a justifiable approach is addressed. For this purpose a simulation of the A2 case is performed on the A1 CAA grid. A juxtaposition of the results as well as the measured data is given in Fig. 11. Despite some minor deviations, both the resolved and unresolved case result in a similar spectrum. However, the resolution of the tip gap might not be sufficient enough in the first place, thus eventuate in a spectrum alike as for the unresolved setup.

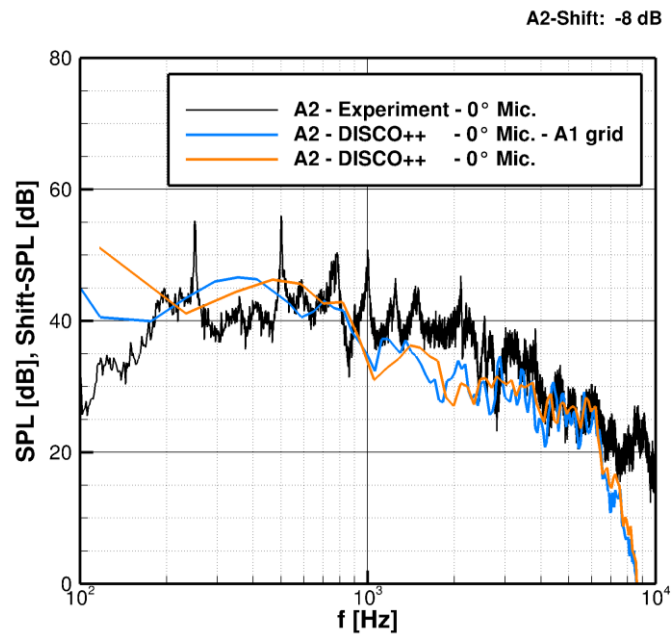


Figure 11: Case A2 simulated with resolved (orange) and unresolved tip gap (blue).

SUMMARY AND CONCLUSION

In the present work the recently developed CAA solver DISCO++ was presented. The numerical method of combining stochastically generated acoustic sources, obtained from a RANS solution, with a discontinuous Galerkin based propagation code to solve the APE was introduced. To validate the noise prediction capabilities of the method a benchmark test case was chosen. Sound generation and propagation of the ducted five bladed axial fan USI7 was computed in a rotating frame of reference without consideration of any upstream environment. Two different configurations of the tip clearance at the ventilator blade were evaluated. The sound pressure level spectra obtained by means of simulation were confronted with measurement data for both cases. A good agreement in the shape of measured and simulated spectra was ascertained for the smaller gap. The broad band component of the spectrum could well be reproduced in terms of spectral shape, while tonal contribution was considered by the computational setup. In case of the larger gap, the simulation underpredicts the expected sound pressure levels in a mid-frequency range. A possible explanation might be a not sufficiently refined CAA grid in the tip gap area. In future studies, the simulation results obtained by DISCO++ should be evaluated further by comparison with other numerical studies [4,5,9], particularly regarding the computational efficiency of the presented method.

BIBLIOGRAPHY

- [1] R. Ewert, W. Schröder – *Acoustic perturbation equations based on flow decomposition via source filtering*, Journal of Computational Physics, 188, **2003**
- [2] A. D. Pierce – *Wave equation for sound in fluids with unsteady inhomogeneous flow*, The Journal of the Acoustical Society of America, 87, **1990**
- [3] W. Möhring, E.-A. Müller, F. Obermeier – *Problems in flow acoustics*, Review of Modern Physics, 55 (3), **1983**
- [4] S. E. P. Bergliaffa, K. Hibberd, M. Stone, M. Visser – *Wave equation for sound in fluids with vorticity*, Physica D, 191, **2004**
- [5] T. Carolus, T. Zhu, M. Sturm – *A low pressure axial fan for benchmarking prediction methods for aerodynamic performance and sound* - Noise Control Engineering Journal, 63 (6), **2015**
- [6] A. Pogorelov, M. Meinke, W. Schröder – *Cut-cell method based large-eddy simulation of tip-leakage flow*, Physics of Fluids, 27, **2015**
- [7] T. Zhu, D. Lallier-Daniels, M. Sanjose, S. Moreau, T. Carolus – *Rotating Coherent Flow Structures as a Source for Narrowband Tip Clearance Noise from Axial Fan*, Journal of Sound and Vibration, 417, **2018**
- [8] R. Ewert – *Broadband slat noise prediction based on CAA and stochastic sound sources from a fast random particle-mesh (RPM) method*, Computers & Fluids, 37, **2008**
- [9] M. Lummer – *A Hybrid 3D Discontinuous Galerkin Code for CAA Applications*, 22nd AIAA/CEAS Aeroacoustics Conference, Lyon, **2016**.
- [10] M. Sturm, M. Sanjose, S. Moreau, T. Carolus – *Aeroacoustic simulation of an axial fan including the full test rig by using the Lattice Boltzmann Method*, Proceedings of Fan 2015 Symposium, Lyon, **2015**
- [11] C. G. Speziale – *Analytical Methods For The Development Of Reynolds-Stress Closures In Turbulence*, Annual Review of Fluid Mechanics, 23 (1), **1991**